Astron. Astrophys. 327, 725–735 (1997)

ASTRONOMY
AND
ASTROPHYSICS

Physical properties of stellar winds from young stellar objects

Hou Jinliang, Jiang Dongrong, and Fu Chengqi

Shanghai Observatory, Chinese Academy of Sciences, Shanghai, 200030, P.R. China (hjlyx@center.shao.ac.cn)

Received 2 April 1996 / Accepted 25 June 1997

Abstract. A non-LTE model for stellar winds from Young Stellar Objects(YSOs) was established. This paper presents the results of an extensive set of calculations. Our basic assumptions in the model are: (a) the central sources are early B-type stars with steady mass loss rates and luminosities in the range of $10^3 \sim 10^4$ solar luminosity; (b) wind has a spherical symmetric geometry and a pure hydrogen composition; (c) the wind has a constant velocity and constant electron temperature. We adopted the Sobolev approximation to treat the line transfer problem. Our calculations indicate that the matter in stellar wind from YSOs deviates strongly from LTE.

We have computed the hydrogen line fluxes and line ratios for a set of model parameters. We find a clear correlation between the line flux ratios of Pfγ/Brα and Brγ/Brα, Paδ/Brα and Brγ/Brα, which are only weakly dependent on the physical conditions of stellar winds and central sources. These relationships can be applied to estimate the foreground extinction of YSOs.

Key words: stars: early-type – infrared: stars – stars: mass loss – radiative transfer – stars: pre-main sequence

1. Introduction

The study of Young Stellar Objects (YSOs) has been one of the topics of interest since the 1980's (Panagia 1991, Yuan and You 1995). Both observation and theory have revealed many important properties of these objects, such as the existence of stellar winds, ionized gas and circumstellar disks (Carr 1989, Henning et al. 1993, Malbet et al. 1993, Nata et al. 1993). These phenomena have significant effects on the evolution of YSOs and the dynamics of their environments.

Most of the YSOs form in large and dense molecular clouds. Due to obstruction by dust, visible observations are difficult. Therefore, the common observations are made using infrared spectroscopy and radio continuum. The first Brα line was obtained by Grasdelen (1976) from BN object in Orion nebula. Since then, Brα, Brγ and Pfγ emission lines with FWHM 100$\sim$200 kms^{-1} have been detected in many YSOs or related ultracompact HII regions with young exciting stars inside (Simon et al. 1983, Persson et al. 1984, Evans et al. 1987, Beck et al. 1991, Doherty et al. 1994, Howard et al. 1996). Under observation, Young Stellar Objects can be distinguished from obscured HII regions and other infrared sources by their infrared continuum shape, their very dense ionized winds, and their association with CO outflow (Evans et al. 1987, Phillips et al. 1988, Lada 1991). On the other hand, different luminosity YSOs will show different physical properties. For low luminosity YSOs, the winds are mostly neutral (Natta et al. 1988). This has been one of the possible explanations for the discrepancy between Brackett line luminosity and mass loss rate deduced from CO observation. Moreover, the infrared spectroscopy has indicated that some of the high luminosity (L$>10^3 L_\odot$) YSOs have large Brackett line FWHM, which suggests that the infrared recombination lines formed in the ionized stellar wind. Also those YSOs have Brγ line strength in excess of the one predicted by Case B recombination theory (Thompson 1984, 1987, Hamann and Persson 1992). Simon et al. (1983) first suggested that the Balmer continuum of a YSO could ionize hydrogen atom from the first excited level and produce enough photons to meet the observed infrared line fluxes. In order to understand the physical properties of YSOs, the infrared line fluxes and ratios have been used to determine the density and temperature (McGregor et al. 1988, Doherty et al. 1996), the abundance and reddening (Kelly et al. 1994, Howard et al. 1996). The reddening corrections from different line ratios were often quite different. This difference has been ascribed to be the different emission locations for various lines, and the limitation of Case B recombination theory. Observations do show that the hydrogen recombination line ratios are inconsistent with optically thin theory (Simon et al. 1983, Evans et al. 1987, Persson et al. 1988, Beck et al. 1991).

Therefore, a more detailed analysis of infrared recombination lines from stellar wind is necessary in order to have a better understanding of YSOs and their surroundings.

In this paper, we established a non-LTE model for stellar winds from high luminosity ($10^3 \sim 10^4$L$_\odot$) YSOs. We mainly concentrated our study on infrared line fluxes and ratios for a set of model parameters. In Sect. 2, we described our basic model, and in Sect. 3, we gave a comparison with a more sophisticated model. In Sect. 4, we compared the calculated line ratios with observations and presented a method for estimating foreground

Send offprint requests to: Hou Jinliang

extinction towards YSOs. We also discussed the possibilities of mass loss rate determination from infrared line observations. Finally, we provided a summary of the main points in Sect. 5.

2. Basic model and calculation technique

2.1. Wind model

We assumed that (a) the central star is a blackbody with a steady mass loss rate $\dot{M}$, radius r_* and temperature T_*, (b) the stellar wind, composed of pure hydrogen, is spherical symmetric and isothermal, (c) the wind matter is in a state of non-LTE, and (d) departure coefficient b_j and ionization degree χ are functions of distance from the central star. The outflow velocity $V(r)$ is supposed to be large enough to make the Sobolev's method applicable for line radiation transfer (Caster 1970). A hydrogen atom is thought to consist of the 20 lowest bound levels without the splitting of sub-levels (for electron density n_e>$10^9 cm^{-3}$) (Drake & Ulrich 1980).

The basic equation for the model is the rate equation(Mihalas 1978). The photoionization is considered only for the first two levels. Furthermore, while treating the continuum intensity, we have adopted a strict formula for the stellar part J_{cs} in the region very close to the stellar surface in order to avoid large error (Fu Chengqi et al. 1993):

$$J_{cs} = \frac{1}{2}\int_{\mu_c}^{1} B_\nu(T_*)e^{-\tau(\mu)}d\mu, \tag{1}$$

where $\tau(\mu) = \int_0^{x_s(\mu)} n_j(x)a_{jc}(\nu)dx$ is the optical depth from the calculated point in the flow to the point on stellar surface in μ direction, and $x_s(\mu) = r\mu[1 - \sqrt{1-(\frac{\mu_c}{\mu})^2}]$ is the distance between these two points.

The diffuse radiation J_{cd} is processed by on-the-spot approximation according to the standard recombination theory (Osterbrock 1989).

When we compute the integrated line flux, the velocity in the light of sight is given by $V(r)\mu = (\frac{\nu}{\nu_0} - 1)c$, where c is the velocity of light, and ν is the frequency. Only those points that are on the iso-velocity surface have contributions to the total flux at a given frequency. The infrared line flux which is integrated up to the radius R is then calculated by the following formula:

$$L_{nn'}(R) = \int_{-\nu_{max}}^{\nu_{max}}\int_0^R I_\nu(p)2\pi p dp d\nu, \tag{2}$$

where $I_\nu(p) = S_{nn'}(1 - exp(-\tau_{nn'}(\nu, p)))$, $p = r_*\sqrt{1-\mu^2}R$, and $\mu = (\frac{\nu}{\nu_0} - 1)\frac{c}{V(r)}$; $S_{nn'}$ is the source function and $\tau_{nn'}$ is the optical depth of spectral line nn'.

2.2. Parameters and computation procedure

Based on the observations, B-type stars with luminosities in the range of $10^3 \sim 10^4$ solar luminosity are chosen as the central sources (Table 1).

In our model, we assumed that the continuum of a YSO is close to that of a ZAMS star of the same luminosity. The parameters of the central stars are cited from Thompson (1984) and are given in Table 1. The continuum photons were calculated by a black body model. In order to estimate the difference of Lyman and Balmer photon numbers between model atmosphere and the black body approximation, we compared their photon numbers under both situations. The ratio of photon numbers between model atmosphere and black body is defined as correction factor. That is, k_{Ly} for Lyman photons and k_{Ba} for Balmer photons (see Table 1). From Table 1, we can see that the Balmer photon numbers are almost the same for both models, while the Lyman photon numbers are overestimated for the black body model. Also, we compared the calculated results with and without the correction factor k_{Ly}. The results show that k_{Ly} will somewhat affect the ionization structure of the wind from YSO because it greatly reduces the ionization photon numbers from the central source, especially for those relatively low luminosity objects. However this has little effect on the infrared line ratios (see below).

We assumed that the wind has a constant velocity of 100$\sim$150 kms^{-1}, which is typical of many YSOs. The mass loss rate $\dot{M}$ was set to be about $10^{-5} \sim 10^{-7} M_\odot yr^{-1}$. Although the wind matter is almost certainly non-isothermal, the isothermal or empirical temperature distribution model is the most commonly used. Here an isothermal model is adopted and the gas temperature T_e is set to be 10^4K.

While solving rate equation, we divided wind matter into about one hundred of thin shells with different thickness. The computation was carried out from the surface of the central star to the outer region one shell after another.

Generally, the calculation is performed up to a fixed radius ($980r_*$). For some parameters shown in Table 2, the wind remained fully ionized within this distance, and for other ones, the ionization fraction decreased with the distance from the central star. R_{out} is the radius where the ionization degree reduces to about 0.5. For all parameters, the volume-integrated line emissivity has already become constant before the distance from the central star reaches $980r_*$.

3. Test calculations of the model

In order to test the reliability of our model calculations, we compared the results of two of our models, B05 central star with $V_*/\dot{M}_{-6}$ equals to 100/1.5 and 100/0.5, with stellar atmosphere calculations. The test code is the non-LTE co-moving frame atmosphere of Hamann & Schmutz (1987). The test calculations have been provided by Schmutz (1996). The model is adjusted to our model parameters, but in addition to the wind, it also includes the transition zone with a velocity law specified by β=1 and hydrostatic layers in the photosphere. Thus, in the test calculations, the full problem of a stellar atmosphere with a spherical expanding envelope is solved consistently.

Fig. 1 shows the dependence of relative population and ionization fraction χ on electron density. Plots (a) and (b) are our results with the parameter for the stellar Lyman photons set

Table 1. Parameters for central stars in the model

Sp	T_*	r_*	$\log(L/L_\odot)$	$\log N_{Ly}$		k_{Ly}	$\log N_{Ba}$		k_{Ba}
	(K)	(10^{11} cm)		Thompson(1984)	B.B.		Thompson(1984)	B.B.	
(1)	(2)	(3)	(4)	(5)	(6)	(7)	(8)	(9)	(10)
B0	30900	3.891	4.40	47.23	47.92	0.20	48.83	48.77	1.15
B0.5	26200	3.467	4.03	46.12	47.32	0.06	48.48	48.44	1.09
B1	22600	3.236	3.70	45.11	46.76	0.03	48.15	48.16	0.97
B2	20500	2.884	3.45	44.45	46.30	0.02	47.91	47.91	1.00
B3	17900	2.291	3.01	43.36	45.45	0.01	47.47	47.49	0.96

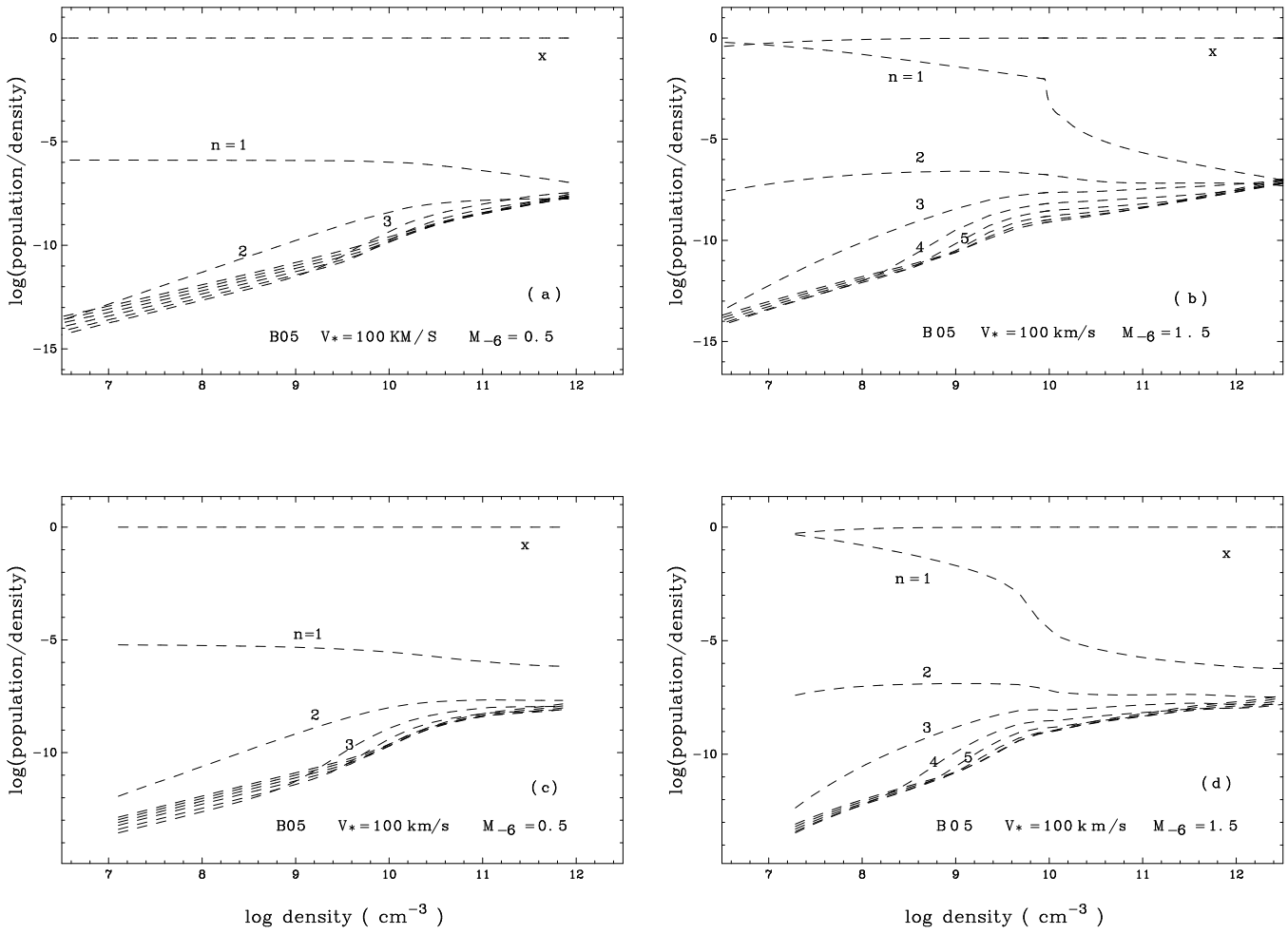

Fig. 1a–d. Dependence of computed relative populations on the electron density (**a**) and (**b**) and comparison with atmospheric model from Schmutz (1996) (**c**) and (**d**) for typical model parameters (see text). The numbers beside each curve represent the hydrogen levels, and χ is the ionization fraction.

to k_{Ly} = 1.0. The plots (c) and (d) are the results from the atmosphere model (Schmutz 1996). The ratios of populations between the two codes are shown in Fig. 2a. These results are quite consistent for population distribution except for the first two levels. The hydrogen recombination radius R_{out}, defined here as the distance where ionization fraction drops to about 0.5, and the ionization fraction also have similar values. The discrepancies are mainly caused by two effects, one is the wind velocity which has some difference in the inner region between the two codes, and the other one is the different temperature structure. In spite of this, the general behaviors of these two results are quite similar as can be seen from Fig. 1.

In Fig. 2b, we also show the difference of our results obtained with k_{Ly} = 0.06 (see Table 1 for the values of k_{Ly} and Sect. 2.2 for the definition of it) with the atmosphere model (Schmutz 1996). The comparison of the test calculations with k_{Ly} = 1 and k_{Ly} = 0.06 clearly demonstrates that with the exception of n =1 in the innermost layers, k_{Ly} = 1.0 is the much

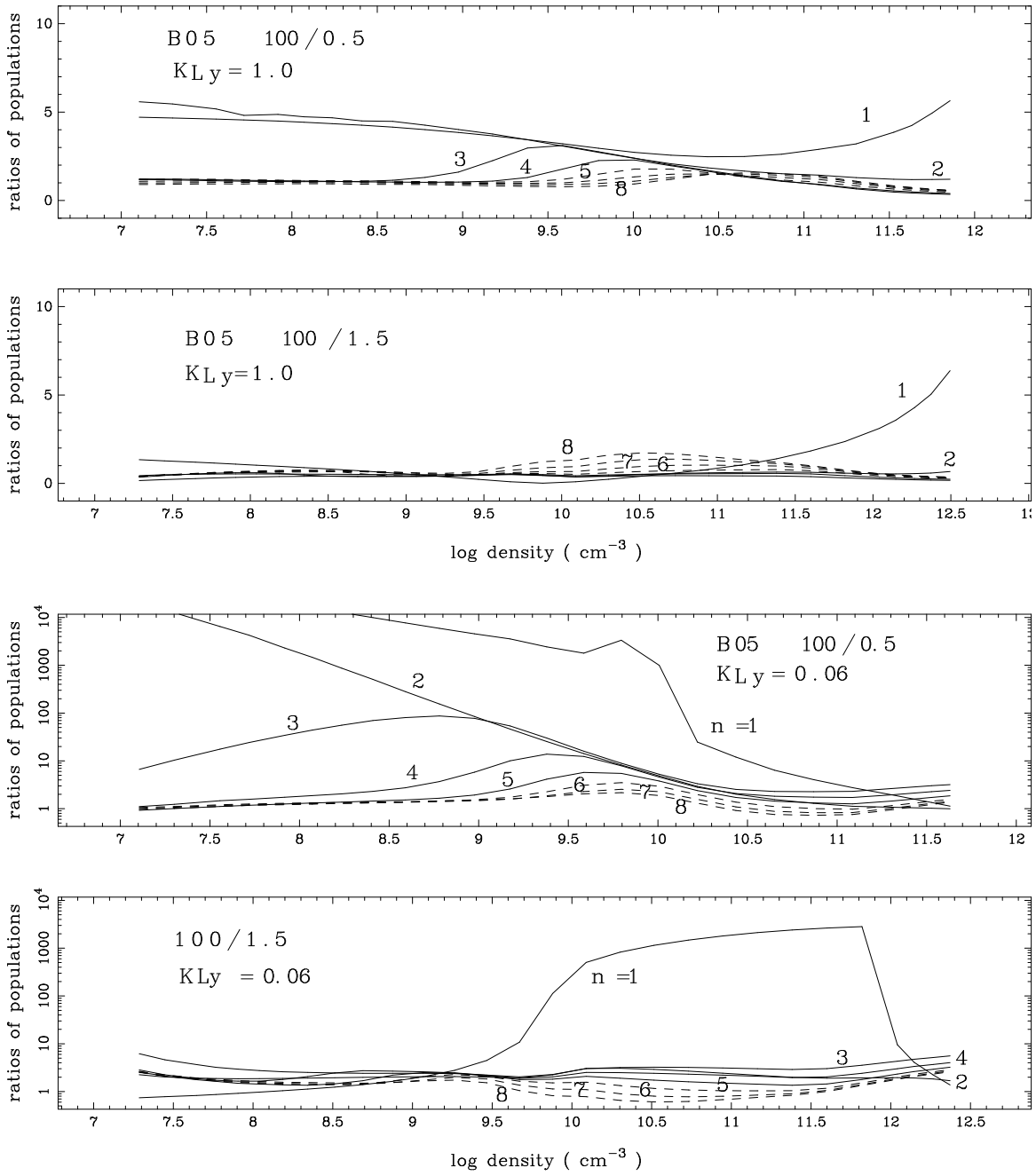

Fig. 2a and b. Ratios of level populations between our model results and Schmutz's model atmosphere (Schmutz 1996). Plot **a** (upper part) is from k_{Ly} = 1 calculation and **b** (lower part) from k_{Ly} = 0.06 situation, where k_{Ly} is the parameter for the number of Lyman photons (see text for the explanation of this parameter). It can be seen that there are much greater differences when introducing a non-unity correction factor.

better approximation. Therefore, we have adopted k_{Ly} = 1 for the calculations presented below.

However, as we have pointed out in Sect. 2.1, our rate equation is most suitable for electron density $n_e \geq 10^9$ cm^{-3}. This sets up the limitation of the choice of model parameters. If the $V_*/\dot{M}_{-6} \sim 10^3$, the electron density will be about 10^8 cm^{-3} at a distance of 100r_*. Therefore, some model parameters in Table 2, such as $V_*/\dot{M}_{-6}$ = 150/0.2 for B05 group, $V_*/\dot{M}_{-6}$ = 100/0.07 for B3 group, are just around the limitation of our approximation. Thus, the calculated line ratios for these parameters will have relatively larger uncertainties.

4. Physical properties of the stellar winds from calculations

Some model parameters ($V_*/\dot{M}_{-6}$) and the results are given in Table 2, where $\dot{M}_{-6}$ is the mass loss rate in unit of $10^{-6} M_\odot yr^{-1}$, R_s refers to the classical $Strömgren$ radius (Osterbrock 1989), R_1 is the radius of the Lyman photon deple-

Table 2. Model parameters and the results of non-LTE calculations for early B type central star.

Sp	$V_*/\dot{M}_{-6}$	R_S	R_1	R_{out}	intrinsic line ratios		
					Brγ/Brα	Pfγ/Brα	Paδ/Brα
(1)	(2)	(3)	(4)	(5)	(6)	(7)	(8)
B0	100/5.0	1.046	3.7	400	0.736	0.219	1.422
B0	100/2.0	1.375	>980	>980	0.931	0.304	2.981
B0	100/1.5	1.942	>980	>980	0.938	0.316	3.061
B0	100/1.0	/	>980	>980	1.020	0.358	3.406
B0	100/0.8	/	>980	>980	1.061	0.382	3.590
B0	100/0.5	/	>980	>980	1.140	0.432	3.934
B0	150/5.0	1.109	13.0	560	0.820	0.247	1.987
B0	150/2.5	1.648	>980	>980	0.963	0.323	3.131
B0	150/1.5	/	>980	>980	1.057	0.377	3.543
B0	150/1.0	/	>980	>980	1.162	0.431	3.964
B05	100/5.0	1.010	1.3	200	0.755	0.220	1.451
B05	100/1.5	1.122	20.0	500	0.880	0.266	2.373
B05	100/0.8	1.618	>980	>980	0.967	0.326	3.118
B05	100/0.5	44.16	>980	>980	1.023	0.357	3.427
B05	150/4.0	1.036	3.5	380	0.795	0.239	1.741
B05	150/2.0	1.159	18.0	440	0.892	0.274	2.536
B05	150/1.0	2.221	>980	>980	1.020	0.353	3.347
B05	150/0.8	7.902	>980	>980	1.051	0.370	3.505
B05	150/0.5	/	>980	>980	1.142	0.415	3.923
B05	150/0.2	/	>980	>980	1.480	0.548	4.596
B1	100/5.0	1.001	1.1	150	0.780	0.225	1.519
B1	100/2.0	1.005	2.2	340	0.770	0.230	1.579
B1	100/1.0	1.022	9.0	400	0.853	0.260	2.273
B1	100/0.2	2.195	>980	>980	1.128	0.392	4.016
B1	100/0.1	/	>980	>980	1.397	0.467	5.641
B1	150/3.0	1.005	2.0	300	0.790	0.239	1.678
B1	150/1.5	1.020	6.2	360	0.882	0.273	2.412
B2	135/5.0	1.001	1.06	120	0.809	0.235	1.629
B2	135/1.0	1.037	3.6	330	0.901	0.277	2.484
B2	135/0.5	1.165	11.0	260	0.973	0.309	2.978
B2	135/0.2	8.650	>980	>980	1.151	0.396	4.020
B2	135/0.1	/	>980	>980	1.401	0.464	5.036
B2	100/0.37	1.165	13.0	300	0.964	0.301	2.957
B2	100/0.15	7.282	>980	>980	1.180	0.398	4.424
B3	150/5.0	1.002	1.01	150	0.898	0.263	1.830
B3	150/1.0	1.006	1.42	230	0.879	0.268	2.160
B3	150/0.5	1.025	2.4	220	0.929	0.294	2.595
B3	150/0.2	1.177	7.2	180	1.083	0.354	3.508
B3	150/0.1	/	>980	>980	1.224	0.408	4.508
B3	100/0.67	1.006	1.5	260	0.840	0.254	1.975
B3	100/0.07	/	>980	>980	1.286	0.422	5.072

tion shell (Jiang et al. 1994), R_{out} is the hydrogen recombination radius. All of the radii are in units of r_*.

Our results show that the wind matter around YSO is far away from LTE. And the lower the level is, the farther the departure from LTE. From Table 2, we see that for early B0, B05 and B1 central stars, the hydrogen recombination distance R_{out} (column 6) has an anti-correlation with mass loss rate for a given wind velocity, that means the distance increases when the mass loss rate decreases. This is consistent with common properties of stellar winds (Schmutz and Hamann 1986). However, we can also see from Table 2 that for B2 and B3 central stars, this behavior does not appear. Since the ionization structure has little effect on the infrared line ratios, we will not consider this phenomena at present.

4.1. Theoretical infrared line fluxes and line ratios

The infrared lines observed towards YSOs are Brα(4.05μm), Brγ(2.17μm) and Pfγ(3.74μm) of hydrogen atom. In some less obscured sources, Paschen lines are also observed. Based on the departure coefficients of the hydrogen levels obtained from various model parameters, we can calculate the line fluxes and ratios for those hydrogen lines according to Eq. (2). The emergent line ratios are given in Table 2.

Fig. 3 gives the product of escape probability β and line emissivity ($erg * cm^{-3} sec^{-1}$) for typical model parameters. Dash lines are the results from Case B theory(Storey and Hummer 1995). Comparison indicates that our results differ considerably from the results of nebular recombination, especially in the high density regions where the high optical depth could prevent any photon from escaping.

In order to analysis the infrared line ratios, we plot in Fig. 4 the line ratios corresponding to each model parameter.

Clearly, there is a correlation between Pfγ/Brα and Brγ/Brα, Paδ/Brα and Brγ/Brα that is nearly independent of the physical conditions of the wind and the central star. The solid curve in Fig. 4 is a least-square fit for the data, where r represents the correlation coefficient. The results of least-square fitting are:

$$Y_1 = -0.099 + 0.429X, \tag{3}$$

$$Y_2 = -2.712 + 5.776X \tag{4}$$

where X = Brγ/Brα, Y_1 = Pfγ/Brα, and Y_2 = Paδ/Brα. The fitted errors for Y_1 and Y_2 are 1.8% and 29%, respectively.

In Fig. 4, the points outside the relation do not reflect statistical scatter but instead reflect different physical conditions. We have isolated a group of parameters corresponding to a fixed spectral type of the central star and then did the fitting. The deviates for fitted results from the mean results are not large, especially for Pfγ/Brα ratio. If we rewrite the Eqs. (3) and (4) as $Y_1 = a_1 + b_1X$, $Y_2 = a_2 + b_2X$, then the maximum relative errors of coefficient b_1 comes from $B0$ central star with an error to the mean relation of about 23%, and for b_2 it comes from $B3$ central star, with an error of about 24%.

We have also computed the line ratios when Lyman photon numbers are corrected by k_{Ly} given in column (7) of Table 1. The values of fitted coefficients in Eqs. (3) and (4) are quite similar, especially for the relationship between Pfγ/Brα and Brγ/Brα. The relative errors for the coefficients in Eqs. (3) and (4) are about 5% and 15%, respectively.

Alonso-Costa and Kwan (1989) (hereafter, A&K) have also studied the dependence of the line ratios on the YSOs luminosity, the distance of the emitting gas from the YSO, and the nucleon density of the gas cloud. The geometry of the circumstellar clouds around a YSO was assumed to be plane-parallel

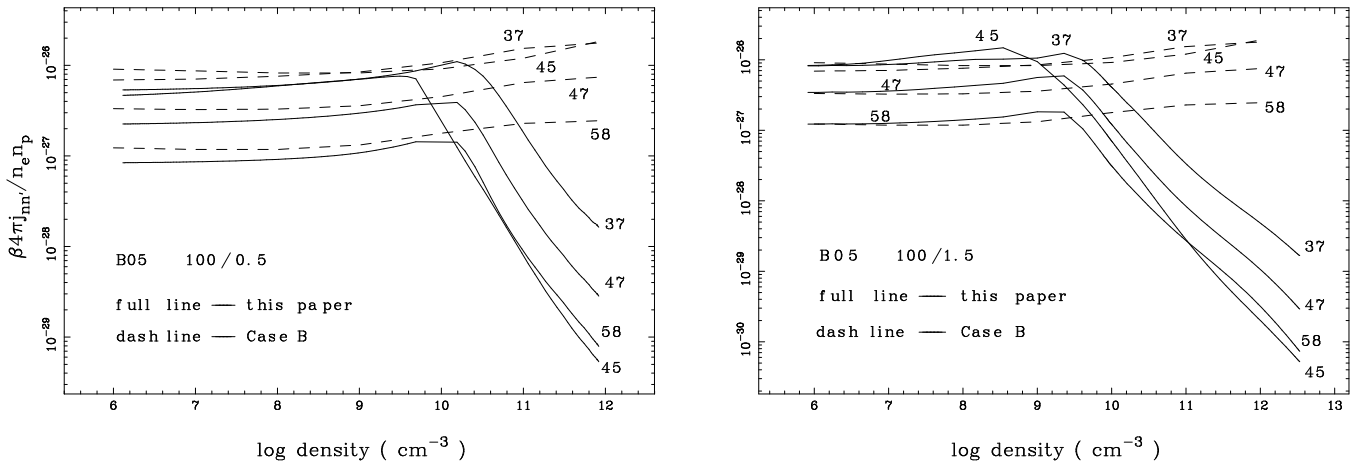

Fig. 3. Infrared line emissivities vs. density and comparison with Case B recombination theory for typical parameters, where β is the escape probability, and the numbers beside the curves represent the infrared line. 37 is Paδ line, 45 is Brα, 47 is Brγ, and 58 is Pfγ line.

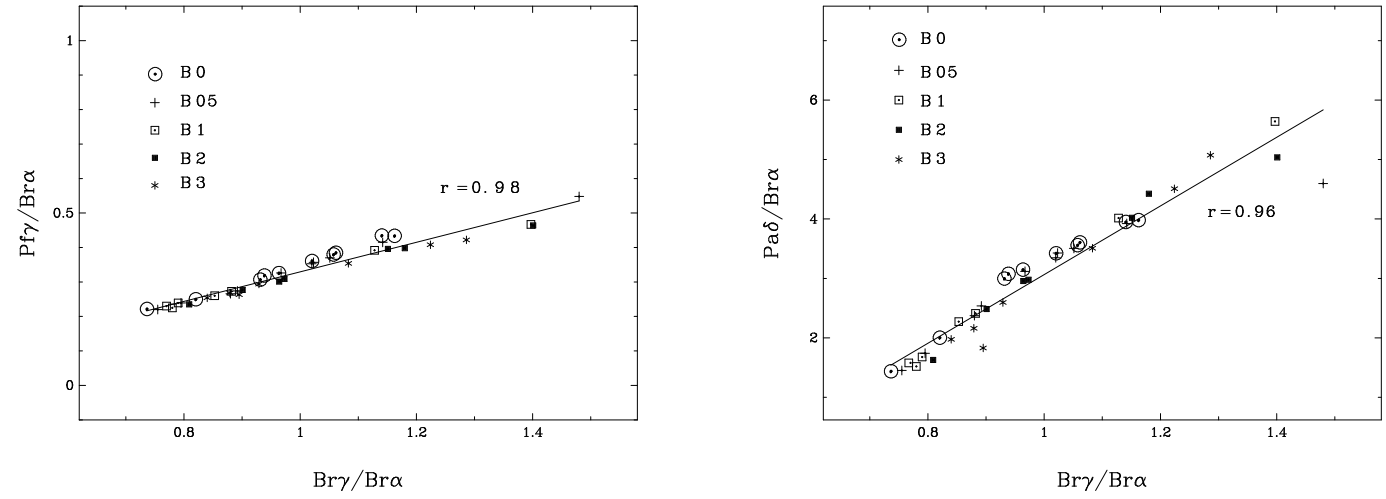

Fig. 4. Theoretical curves of Pfγ/Brα vs. Brγ/Brα and Paδ/Brα vs. Brγ/Brα, where r is the correlation coefficient.

with thickness $l \leq r/3$, where r is the distance from the YSO. The gas cloud is moving away from the YSO. This is quite different from our model in geometry, but they also showed that there is a strong correlation between Pfγ/Brα and Brγ/Brα that is nearly independent of the physical conditions of the emitting region. The derived line ratio Pfγ/Br$\gamma \sim 0.35$. If we omit the constant term in our Eq. (3), we can obtain Pfγ/Br$\gamma \sim 0.43$. The relative error with the result of A&K is about 20%. Both models show the weak dependent of line ratios on model parameters.

From Fig. 4, we see that the values of Brγ/Brα are in the range of $0.74 \sim 1.5$, Pfγ/Brα of $0.21 \sim 0.55$. For many infrared sources with early B-type ZAMS central stars, the observed Brγ/Brα line ratios have values of $0.1 \sim 1.0$, Pfγ/Brα values of $0.10 \sim 0.26$. If corrected by foreground extinction, the observed values are comparable to our model calculations. This cannot be understood by Case B recombination theory which gives: (1) the maximum intrinsic Brγ/Brα values of about 0.54 (2) the maximum intrinsic Pfγ/Brα values of about 0.19 both at n_e=10^{10} cm^{-3} and T$_e$=10^4K (Storey and Hummer 1995).

4.2. Foreground extinction estimation

In order to understand the physical properties of the deeply embedded YSOs, it is very important to precisely estimate the foreground extinction towards those objects. Early attempts to estimate the visual extinction were based on the classical recombination theory. With the assumption of optically thin Bracket line and radio emission, there are two ways to estimate the extinction. For an assumed electron temperature and H^+-to-He^+ ratio, the radio flux density from the same region can be used to give a prediction of the intrinsic, unreddened Brα and Brγ line fluxes. Comparing the observed Brackett measurement with the prediction gives an extinction measure. By contrast, if an extinction law is assumed, the Brα to Brγ ratio can be used to

Table 3. Foreground extinctions for some YSOs from infrared line ratios.

IR Sources	Sp	IR line flux($10^{-15}W/m^2$)			IR	A_V		
		Brα	Brγ	Pfγ	Ref.	this paper	others	A_V ref.
(1)	(2)	(3)	(4)	(5)	(6)	(7)	(8)	(9)
NGC6334 IRS1	B0	11.0	0.33	2.0	(1)	55.6±4.9	50	(4)
Mon R2 IRS1	B0	17.4	1.6	2.1	(1)	30.7±5.0	23	(5)
MWC297	B0	61.4	44.2	15.6	(2)	2.5 ±4.8	2.9	(6)
R Mon	B0	3.33	1.02	0.48	(2)	11.1±5.0	3.6	(7)
S106IRS4	B05	25.0	5.3	3.5	(1)	17.3±5.0	21	(5),(8)
LkHα101	B05	160	34	25	(1)	18.5±5.0	16	(9)
GL961	B1	8.0	1.0	1.7	(1)	31.8±4.9	>15	(10)
MWC1080	B1	2.6	2.6	1.1	(1)	4.0 ±4.7	5.4	(11)
BN	B2	18.0	1.9	3.4	(1)	33.4±4.9	25-50	(12)
M17 IRS1	B2	5.4	1.5	1.4	(1)	20.0±4.9	15	(5)
HD200775	B3	7.96	5.05	1.47	(2)	0.8 ±5.0	1.8	(2)
CRL490	B3	3.2	0.7	1.32	(3)	33.2±4.9	14-50	(3),(7),(13)

References: (1) Alonso-Costa and Kwan 1989; (2) Nisini et al. 1995; (3) Persson et al. 1988;
(4) Davis and Eisloffel 1995; (5) Simon et al. 1983; (6) Berrilli et al. 1992; (7) Kelly et al. 1994;
(8) Felli et al. 1985; (9) Rudy et al. 1991; (10) McGreger et al 1984; (11) Cohen and Kuhi 1979;
(12) Thompson and Tokunaga 1979a; (13) Campbell et al. 1986

Table 4. The de-reddened line ratios and deduced $\dot{M}_{-6}/V_*$.

IR Sources	Sp	observed line ratios		A_v	A_v	dereddened line ratios		$\dot{M}_{-6}/V_*$		
		Brγ/Brα	Pfγ/Brα	(mag)	ref.	Brγ/Brα	Pfγ/Brα	A	B	mean
(1)	(2)	(3)	(4)	(5)	(6)	(7)	(8)	(9)	(10)	(11)
IRAS 12389-6147	B0	...	0.34	21.0	(1)	...	0.37	...	1.0^{-2}	1.0^{-2}
M8EIR	B0	0.29	...	15.0	(2)	0.69	...	e	...	...
MWC349	B0	0.43	...	8.8	(3)	0.72	...	6.7^{-2}	...	6.7^{-2}
NGC6334 IRS1	B0	0.03	0.18	55.6	(T)	0.77	0.23	4.5^{-2}	4.5^{-2}	4.5^{-2}
Mon R2 IRS1	B0	0.09	0.12	30.7	(T)	0.55	0.14	e	e	...
R Mon	B0	0.31	0.14	11.1	(T)	0.59	0.15	e	e	...
MWC297	B0	0.72	0.25	2.5	(T)	0.83	0.26	3.0^{-2}	3.0^{-2}	3.0^{-2}
S106IRS3	B05	0.21	0.14	17.3	(T)	0.58	0.15	e	e	...
LkHα101	B05	0.21	0.16	18.5	(T)	0.63	0.17	e	e	...
GL961	B1	0.13	0.21	31.8	(T)	0.79	0.24	2.2^{-2}	2.0^{-2}	2.1^{-2}
MWC1080	B1	1.00	0.42	4.0	(T)	1.23	0.43	1.4^{-3}	1.2^{-3}	1.3^{-3}
Z CMa	B1	0.61	...	2.8	(4)	0.72	...	4.2^{-2}	...	4.2^{-2}
IRAS07173-1733	B2	1.10	0.34	2.0^a	(1)	1.24	0.35	0.8^{-3}	2.1^{-3}	1.4^{-3}
BN	B2	0.11	0.19	33.4	(T)	0.74	0.22	4.8^{-2}	4.2^{-2}	4.4^{-2}
M17 IRS1	B2	0.28	0.26	20.0	(T)	0.89	0.28	1.1^{-2}	0.8^{-2}	0.9^{-2}
CRL490	B3	0.19	0.42	33.2	(T)	1.35	0.48	e	e	...
NGC2024 IRS2	B3	0.25	...	21.5	(5)	0.87	...	1.3^{-2}	...	1.3^{-2}
S235B	B3	0.49	...	8.4	(2)	0.79	...	3.2^{-2}	...	3.2^{-2}
LkHα198	B3	0.67	...	4.5	(6)	0.89	...	1.0^{-2}	...	1.0^{-2}
HD200775	B3	0.63	0.18	0.8	(T)	0.67	0.19	e	e	...

A, B in column (9) and (10) represet results from Brγ/Brα, Pfγ/Brα respectively.
a : for this source, the iteration cannot converge, so the A_v was from Beck et al. 1991
e : de-reddened line ratios exceeds the acceptable range for applying Eq.(6) (see text for detail).
References: (T) This paper; (1) Beck et al. 1991; (2) McGreger et al. 1984; (3) Cohen et al. 1985;
(4) Berrilli et al. 1992; (5) Jiang et al. 1984; (6) Cohen and Kuhi 1979

give an estimation of the extinction (Herter et al. 1981, Howard et al. 1996). Observations and theoretical calculations have already shown that the classical nebular theory may not hold for emission regions around YSOs. This will result in incorrect extinction estimates for some sources. Our non-LTE model calculations also indicate that the hydrogen lines are optically thick for the majority of the wind parameters.

Using Landini's(1984) monochromatic extinction law:

$$A_\lambda = 0.75 A_V [0.7/\lambda(\mu m)]^{1.85}, \quad 0.7(\mu m) < \lambda < 5.0(\mu m) \quad (5)$$

where A_V is visual extinction and A_λ is the extinction (in magnitude) at wavelength λ (μm), we could derive the visual extinction based on Eq. (3) or (4) as long as three line fluxes are available.

Table 3 gives our A_v estimations for some YSOs and infrared sources. The determined A_v is generally agree with those estimated by other methods. The main difference may be caused by the simplification of our model and also by the different observed line spectra. The given errors are internal errors, where we have assumed that the observed line flux has an error of 20%. Another internal error comes from the fitted error. The shorter infrared wavelength lines, such as Paschen series, may form in the outer region compared with those longer wavelength as Brackett lines. Thus, the extinction derived from longer wavelength line may be larger than those from shorter lines (Evans et al. 1987, Kelly et al. 1994). Here, we have combined three line ratios so that we can derive a sole visual extinction value. However, only a limited number of infrared sources have well observed Brackett and Pfund line fluxes and also well established values of A_v. It is necessary to measure those lines for a large number of sources in order to validate the theoretical relations.

4.3. The possibility of determining the mass loss rate from YSOs

Mass loss is a common phenomena for early-type stars. Derivation of mass loss rate for those objects would be important in many respects. In modeling stellar wind, the mass loss rates are of prime importance to those studying the interaction between central sources and molecular clouds. The mass loss will also affect the evolution of luminous central early-type stars. In early years, the observations of infrared excess, UV resonance lines and Hα emission are the bases for mass loss rate determination. Since the discovery of the association between molecular outflows and their central sources (Lada 1985), the radio observations to the outflows provide a new approach to the mass loss problem (Leverault 1988). Generally speaking, the infrared line alone is not possible to derive the mass loss rate because the mass loss rate is not the only parameter that determines the line strengths. In addition, the knowledge of temperature and luminosity of the central star is required (Schmutz et al. 1989).

In the present model, we have assumed that the YSOs have the same parameters (radius, temperature and luminosity) as ZAMS. Under such an assumption or if we could really obtain the properties for a specific YSO, the line ratios might provide a possible route to derive the mass loss rate.

Table 5. The mass loss rate deduced from $\dot{M}_{-6}/V_*$

Sources	wind velocity		$\dot{M}_{-6}(10^{-6} M_\odot yr^{-1})$		
	(kms^{-1})	Ref.	this paper	others	$\dot{M}$ Ref.
(1)	(2)	(3)	(4)	(5)	(6)
IRAS 12389-6147	150	(1)	1.5	2.7	(1)
M8EIR	235	(2)	...	0.78	(2)
MWC349	103	(3)	6.7	...	
NGC6334 IRS1	70	(4)	4.5	...	
Mon R2 IRS1	70	(2)	...	0.80	(2)
R Mon	225	(2)	...	0.16	(2)
	170	(5)	...	0.014	(5)
MWC297	100	a	3.1	1.4	(5)
S106IRS3	125	(6)	...	0.5	(12)
				2.0	(2)
				3.8	(13)
LkHα101	60	(2)	6.0	4.7	(2)
	350	(7)	35.0	11	(7)
				44	(14)
GL961	75	(2)	1.6	0.77	(2)
MWC1080	500	(8)	0.7	1.7	(8)
	1000	(9)	1.4	1.1	(5)
Z CMa	620	(10)	25.0	300	(15)
IRAS07173-1733	230	(1)	0.26	0.28	(1)
BN	80	(2)	3.5	0.8	(2)
				14.0	(13)
M17 IRS1	135	(2)	1.3	2.2	(2)
CRL490	160	(6)	...	0.45	(2)
NGC2024 IRS2	100	(11)	1.3	0.5	(12)
S235B	100	a	2.9	...	
LkHα198	100	a	1.0	0.32	(16)
				5.0	(11)
HD200775	145	(5)	...	0.14	(5)
				0.24	(8)

a: velocity assumed to be 100 kms^{-1}

References: (1) Beck et al. 1991; (2) Persson et al. 1984; (3) Hamman and Simon 1986;
(4) Davis and Eisloffel 1995; (5) Skinner et al. 1993; (6) Persson et al. 1988,
(7) Barsony et al. 1990; (8) Skinner et al. 1990; (9) Yoshida et al. 1992;
(10) Poetzel et al.1989; (11) Chalabaev and Lena 1986; (12) Chandler et al. 1995;
(13) Carr 1989; (14) Cohen et al. 1982; (15) Hartmann et al. 1989;
(16) Evans et al. 1987

For the parameters we explored in the model, there exist monotonic relationships between $\dot{M}_{-6}/V_*$ and a pair of infrared line ratios (Brγ/Brα, Pfγ/Brα and Paδ/Brα) for a specific central star (Fig. 5). If we have the observed Brγ/Brα or Pfγ/Brα or Paδ/Brα line ratio, and correct extinction towards central source, then the unreddened line ratios could be obtained. Thus, the $\dot{M}_{-6}/V_*$ values could be determined by assuming the spectral type of the central source and using the relationship derived from our model calculations. Therefore, it is possible to derive the mass loss rate because the terminal wind velocity could be measured by velocity-resolved infrared spectroscopy.

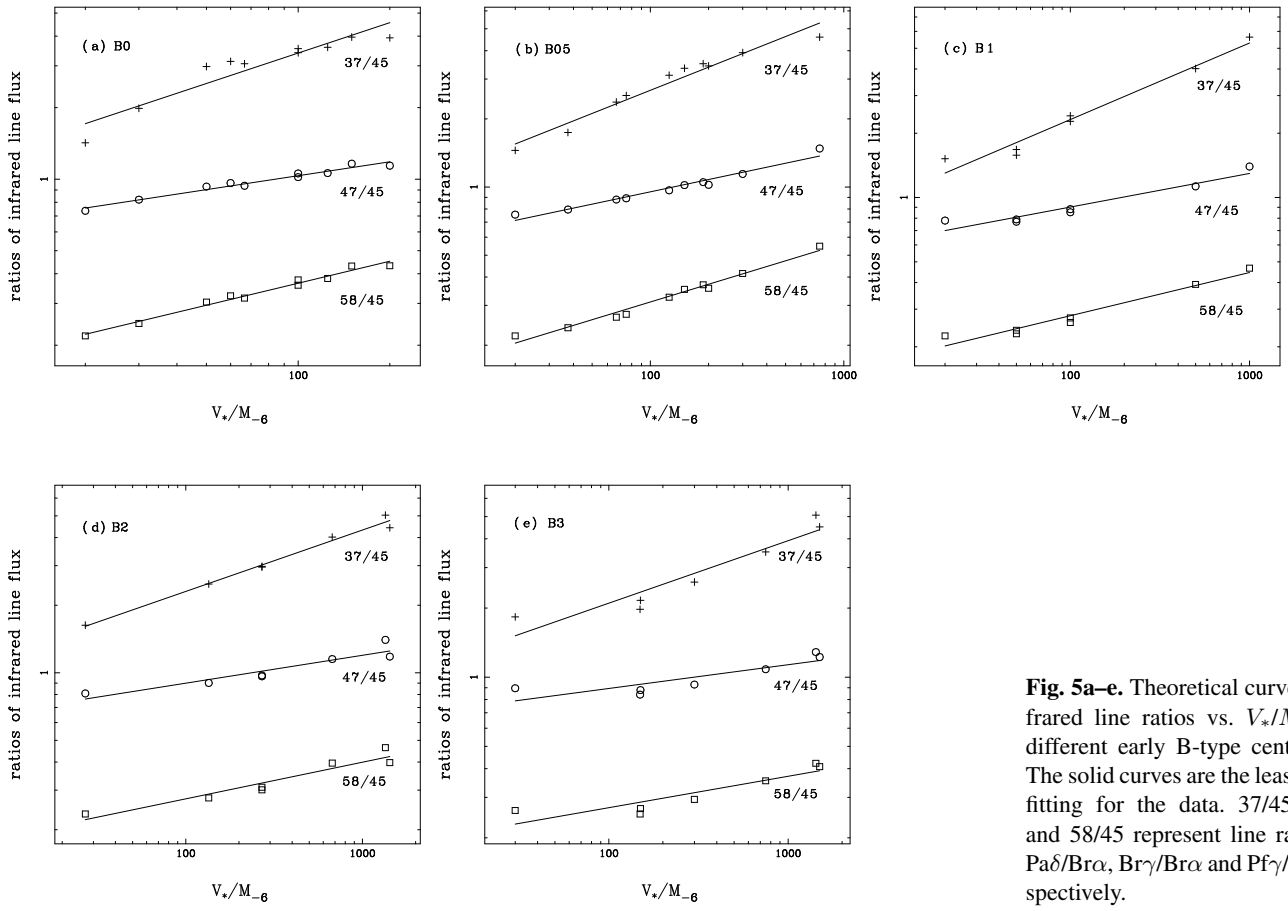

Fig. 5a–e. Theoretical curves of infrared line ratios vs. $V_*/\dot{M}_{-6}$ for different early B-type central star. The solid curves are the least square fitting for the data. 37/45, 47/45 and 58/45 represent line ratios for Paδ/Brα, Brγ/Brα and Pfγ/Brα, respectively.

Fig. 5a-e gives the relationship between $V_*/\dot{M}_{-6}$ and infrared line ratios $L_{n_1n_2}/L_{45}$ for different central sources, where n_1, n_2 represent the lower and upper levels of transition. L_{45} is the flux of Brα line. The numbers beside every solid line represent the ratio of two lines (47/45 means Brγ/Brα etc.). We suggest that the relationship is:

$$log(L_{n_1n_2}/L_{45}) = a_{n_1n_2} + b_{n_1n_2} log(V_*/\dot{M}_{-6}) \quad (6)$$

where $a_{n_1n_2}$,$b_{n_1n_2}$ are fitted coefficients for various central stars. The acceptable range for applying Eq. (6) is given by the range of mass loss rate and wind velocity comprised by our models. If the derived value of $V_*/\dot{M}_{-6}$ is outside the valid range we have not attempted to calculate a mass loss rate. This is indicated by e in column 9 and 10 of Table 4.

Column (4) in Table 5 is the derived mass loss rate for some YSOs and infrared sources compiled from literature, where the majorities of wind velocities are from infrared spectroscopy. Column (5) gives the mass loss rates from literature. Although there are larger differences for some specific sources, the general agreement is quite satisfactory. The mass loss rates from literature are mostly derived from radio and CO observations. The results for the same source were often quite different with various techniques and different authors. Moreover, the simplification of the present model can cause errors for the derived mass loss rate. The errors are mainly from the uncertainties of temperature structure, the assumed luminosity of a central star, and also the fitted errors of Eq. (6). However, it is clear that if the physical properties of a YSO could be determined, then it is possible to derive the $\dot{M}_{-6}/V_*$ for that object from the infrared line ratios.

5. Summary

In this section, we summarize the main results of this paper.

1) although our non-LTE model does not include the photosphere of the central star, our approximations are quite good in comparison with the more detailed code of Schmutz (1996) which has included the photosphere of the star while solving the expanding atmosphere.

2) for model parameters, our calculations show that the wind materials around YSOs are far away from the LTE state. The departure coefficients of the lower hydrogen levels deviate from LTE more seriously. They also have radial distributions. The infrared line emissivities derived from the model are generally inconsistent with Case B recombination theory under present conditions, especially in the high density regions. This implies that for high luminosity YSOs($10^{3-4} L_\odot$), Case B theory should not be used while explaining the observed infrared line ratios for those luminous YSOs.

3) Alonso-Costa and Kwan (1989) showed that the relationship of line ratios between Pfγ/Brα and Brγ/Brα was only weakly relied on the model parameters. Our non-LTE model calculations still yield this conclusion (the difference is about 20%). Moreover, we further showed that the correlation also exists for another pair of infrared line ratios (Paδ/Brα and Brγ/Brα). The two relations provide us an alternative way of estimating foreground visual extinction towards YSOs.

4) Schmutz et al. (1989) has already pointed out that the emergent line equivalent width remains constant if the quantity $\dot{M}/V_\infty/R_*^{3/2}$ is kept constant for WR stars. Our model calculations show that if the radius or the luminosity of a YSO could be know, then there exists correlation between line ratios and $\dot{M}/V_*$. A more definite relation of the mass loss rate to line ratios would require a modeling of each individual YSO that makes uses of intensities and profiles of several hydrogen lines.

5) Infrared line measurements are very important for the study of YSOs. Compared with continuum spectra, lines have the great advantage of carrying information about the velocity field of the wind and the possible location of the emitting gas. However, for a YSO, not only the origin of the wind but also the origin of the observed infrared emission lines is still an open question. The emission lines may come from the stellar wind and could also result from the circumstellar matter or mass inflow. In our present model, we intrinsically assumed that the infrared line emissions originated from stellar winds. Additionally, another basic assumption is that the mass loss process is steady with time. In fact, the variability is an observed fact for many YSOs, but the nature and the origin of the variability still need to be understood. Within the framework of spherical symmetric wind, steady mass loss process and constant wind temperature, we have obtained a special relationship between different infrared line ratios. If the outflow is not spherically symmetric, Panagia (1991) has shown that only highly anistropic structure can give results that appreciably deviate from the predictions of the spherically symmetric models. However, because there are many indications of disk mass outflows for YSOs (Reynolds 1986, Pudritz et al. 1991), it is necessary to establish models with asymmetric geometry.

Acknowledgements. The authors wish to thank professor Song Guoxuan and Dr. Drew for reading and correcting the manuscript. Special thanks is given to Dr. W. Schmutz for providing us with the results from his model calculations. We are also grateful to his valuable comments and suggestions while doing model calculations. The author would also thank Professor P.J. Storey for providing his latest results about Case B recombination theory. This research was supported in part by a grant from the National Natural Science Foundation of China and in part by the grant from Astrophysical Branch of Chinese Astronomical Committee.

References

Alonso-Costa J.L. and Kwan J., 1989, ApJ 338,403
Barsony M., Scoville N.Z., Schombert J.M., Claussen M.J., 1990, ApJ 362,674
Beck S.C., Fischer J., Smith H.A., 1991, ApJ 383,336
Berilli F., Corciulo G., Ingrosso G. et al., 1992, ApJ 398,254
Campbell B., Persson S.E., McGregor P.J., 1986, ApJ 305,336
Carr J.S., 1989, ApJ 345,522
Caster J.J., 1970, MNRAS 149,111
Chalabaev A., Lena P., 1986, A&A 168,L7
Chandler C.J., Carlstrom J.E., Scoville N.Z. 1995, ApJ 446,793
Cohen M., Bieging J.H., Dreher J.W., Welch W.J., 1985, ApJ 292,249
Cohen M., Bieging J.H., Schwartz P.R., 1982, ApJ 253,707
Cohen M., Kuhi L.V., 1979, ApJS 41,743
Davis C.J., Eisloffel , 1995, A&A 300,951
Doherty R.M., Puxley P., Doyon R., Brand P.W.J.L., 1994, MNRAS 266,497
Drake S.A., Ulrich R.K., 1980, ApJS 42,351
Evans II N.J., Leverault R. M., Beckwith, S., Skrutskie M., 1987, ApJ 320,364
Felli M., Panagia N., 1981, A&A 102,424
Felli M., Simon M., Fischer J., Hamman F., 1985, A&A 145,305
Fu C.Q., Jiang D.R., Hou J.L., 1993, the Ann. of Shanghai Astron. Obs
Grasdalen G.L., 1976, ApJ Lett. 205,L83
Hamann F., Persson S.E., 1992, ApJ 394,628
Hamann F., Schmutz W., 1987, A&A 174,173
Hamann F., Simon M., 1986, ApJ 311,929
Hartmann L., Kenyon S.J., Hewett R. et al., 1989, ApJ 338,1001
Henning Th., Pfau W., Zinnecker H. and Prusti T., 1993, A&A 276,129
Herter T, 1981, ApJ 250,186
Howard E.M., Pipher J.L., Forrest W.J., De Pree C.G., 1996, ApJ 460,744
Jiang D.R., Hou J.L., Fu C.Q., 1994, Science in China(series A) Vol.37, No.7,850
Jiang D.R., Perrier C., Lena P., 1984, A&A 135,249
Kelly D.M., Rieke G.H., Campbell B., 1994, ApJ 425,231
Kwan J., Alonso-Costa J.L., 1988, ApJ 330,870
Lada C.J. 1991, in C.J. Lada, N.D. Kylafis (eds.), The Physics of Star Formation and Early Stellar Evolution. Kluwer, Dordrecht, p.329
Lada C.J., 1985, ARA&A 23,267
Lamers H.J.G.L.M., Snow T.P., Lindholm D.M., 1995, ApJ 455,269
Landini M., Natta A., Oliva E., Salinan P., Moorwood A.F.M. 1984, ApJ 134,284
Levreault R.M., 1988, ApJ 330,897
Malbet F., Rigant F., Bertout C., Lena P., 1993, A&A 271, L9
McGregor P.J., Hyland A.R., Hillier D.J., 1988, ApJ 324,1071
McGregor P.J., Persson S.E., Cohen J.G., 1984, ApJ 286,609
Mihalas, 1978, Stellar Atmosphere, P127
Natta A., Giovanardi, C., Palla F., 1988, ApJ 332,921
Natta A., Palla F., Butner H.M., Evans N.J., Harvey P.M., 1993, ApJ 406,675
Nisini B., Milillo A., Saraceno P., Vitali F., 1995, A&A 302,169
Oliva E., Moorwood A.F.M., 1986, A&A 164,104
Osterbrock D.E., 1989, Astrophysics of Gaseous Nebulae and Active Galactic Nuclei, University Science Books, California
Panagia N. 1991, in: NATO ASI, The Physics of Star Formation and Early Stellar Evolution. ed. C.J. Lada & N.D. Kylafis (Dordrecht:Kluwer), 565
Pauldrach A.W.A. Puls J., 1990, A&A 237,409
Persson S.E., Geballe T.R., McGregor P.J., Edwards S., Lonsdale C.J., 1984, ApJ 286,289
Persson S.E., McGregor P.J., Campbell B., 1988 ApJ 326,339
Phillips J.P., White G.J., Rainey R. et al., 1988, A&A, 190,289
Poetzel R., Mundt R., Ray T.P., 1989, A&A 224,613
Pudritz R.E., Pelletier G., Gomez de Castro A.I., in: NATO ASI, The Physics of Star Formation and Early Stellar Evolution. ed. C.J. Lada & N.D. Kylafis (Dordrecht:Kluwer), 539

Reynolds S.P., 1986, ApJ 304,713
Rudy R.J., Erwin P.,Rossano G.S., Puetter R.C., 1991, ApJ 383,344
Schmutz W., 1996, private communications
Schmutz W., Hamann W.R., 1986, A&A 166,L11
Schmutz W., Hamann W.R., Wessolowski U., 1989, A&A 210,236
Simon M., Felli M., Cassar L., Fischer J., Massi M., 1983, ApJ 226,623
Skinner S.L., Brown A., Linsky J.L., 1990, ApJ 357,L39
Skinner S.L., Brown A., Stewart R.T., 1993, ApJS 87,217
Storey P.J., Hummer D.G., 1995, MNRAS 272,41
Thompson R.I., 1987, ApJ 312,784
Thompson R.I., 1984, ApJ 283,165
Thompson R.I., Tokunaga A.T., 1979a, ApJ 229,153
Welty A.D., Strom S.E., Edwards, S., Kenyon S.J., Hartmann L., 1992, ApJ 397,260
Wynn-Williams C.G., 1982, Infrared Hydrogen Emission from HII Regions and 'Protostars'. In: Kessler M.F., Phillips J.P(eds.) Proc. XVIth ESLAB Symposium, Galactic and Extragalactic IR Spectroscopy. D. Reidal, Netherlands, p.133
Wynn-Williams C.G., Becklin E.E., 1974, PASP 86,5
Yoshida S., Kogure T., Wakano M., Tatematsu K., Wiramiharadja S., 1992, PASJ 44,77
Yuan Chi and You Junhan eds. 1995, Molecular clouds and star formation, Proceedings of the 7th Guo Shujing Summer School on Astrophysics. 30 June-5 July, 1993, Wuxi, China

This article was processed by the author using Springer-Verlag LaTeX A&A style file *L-AA* version 3.